energies

Article

On the Wind Turbine Wake and Forest Terrain Interaction

Shyuan Cheng [1], Mahmoud Elgendi [2,3,4], Fanghan Lu [1] and Leonardo P. Chamorro [1,4,5,6,*]

1 Department of Mechanical Science and Engineering, University of Illinois, Urbana, IL 61801, USA; shyuanc2@illinois.edu (S.C.); fanghan3@illinois.edu (F.L.)
2 Department of Mechanical Power Engineering and Energy, Minia University, Minia 61519, Egypt; mahgendi@mu.edu.eg
3 Department of Mechanical Engineering, UAE University, Al Ain City P.O. Box 15551, United Arab Emirates
4 Department of Aerospace Engineering, University of Illinois, Urbana, IL 61801, USA
5 Department of Civil and Environmental Engineering, University of Illinois, Urbana, IL 61801, USA
6 Department of Geology, University of Illinois, Urbana, IL 61801, USA
* Correspondence: lpchamo@illinois.edu; Tel.: +1-217-300-7023

Abstract: Future wind power developments may be located in complex topographic and harsh environments; forests are one type of complex terrain that offers untapped potential for wind energy. A detailed analysis of the unsteady interaction between wind turbines and the distinct boundary layers from those terrains is necessary to ensure optimized design, operation, and life span of wind turbines and wind farms. Here, laboratory experiments were carried to explore the interaction between the wake of a horizontal-axis model wind turbine and the boundary layer flow over forest-like canopies and the modulation of forest density in the turbulent exchange. The case of the turbine in a canonical boundary layer is included for selected comparison. The experiments were performed in a wind tunnel fully covered with tree models of height $H/z_{hub} \approx 0.36$, where z_{hub} is the turbine hub height, which were placed in a staggered pattern sharing streamwise and transverse spacing of $\Delta x/d_c = 1.3$ and 2.7, where d_c is the mean crown diameter of the trees. Particle image velocimetry is used to characterize the incoming flow and three fields of view in the turbine wake within $x/d_T \in (2, 7)$ and covering the vertical extent of the wake. The results show a significant modulation of the forest-like canopies on the wake statistics relative to a case without forest canopies. Forest density did not induce dominant effects on the bulk features of the wake; however, a faster flow recovery, particularly in the intermediate wake, occurred with the case with less dense forest. Decomposition of the kinematic shear stress using a hyperbolic hole in the quadrant analysis reveals a substantial effect sufficiently away from the canopy top with sweep-dominated events that differentiate from ejection-dominated observed in canonical boundary layers. The comparatively high background turbulence induced by the forest reduced the modulation of the rotor in the wake; the quadrant fraction distribution in the intermediate wake exhibited similar features of the associated incoming flow.

Keywords: forest effects; turbulence; wind turbine; wake

Citation: Cheng, S.; Elgendi, M.; Lu, F.; Chamorro, L.P. On the Wind Turbine Wake and Forest Terrain Interaction. *Energies* **2021**, *14*, 7204. https://doi.org/10.3390/en14217204

Academic Editor: Andrzej Bielecki

Received: 18 October 2021
Accepted: 31 October 2021
Published: 2 November 2021

1. Introduction

Wind energy has become a competitive contributor in the energy portfolio, and, as a consequence, it has experienced monotonic growth. Future developments are expected to occur in complex topographic and harsh environments due to reduced advantageous sites. Characterization of wind turbines operating in difficult terrains requires significant attention [1]. Particular scenarios include wind turbines operating in forest terrains. There, the interaction of multiple wakes with the canopy can result in turbulent exchange that may modulate the local ecological equilibrium and climate and the performance of large arrays of turbines.

Characterization of coherent motions in boundary layer flows developed over forestry, and vegetative canopies, have been of high relevance over past decades due to their impact on mass, momentum, and energy exchange in the mixing process [2–4]. Proposed by Lu and Willmarth [5], quadrant analysis has been an instrumental tool to quantify the impact on momentum transfer from coherent motions and has been applied in many related phenomena, including flow over various vegetation canopies [6–9]. Yue et al. [10] and Poggi et al. [7] showed that rigid canopies exhibit a predominance of sweeps within the canopy that evolves to ejection dominated away from the canopy tip for a range of Reynolds numbers. Field measurements over forest by Arnqvist et al. [11] showed that coherent structures are dominated by large-scale mixing processes; they also found that local upwind and topography heterogeneity in a forest only have a minor effect on the measured wind statistics. Numerical simulations, e.g., [12,13], and experiments, e.g., [14,15], have provided substantial insight on the dominant motions induced from the mixing layer in relatively dense canopies. The mixing layer dynamics reduce as the density of canopy decreases [16,17] and velocity fluctuates [18]. The distinct structure of the turbulence above forest canopies may strongly modulate turbines' performance and wake; its impacts on the performance and unsteady loading, among others, on wind turbines remain as open problems.

Numerical and experimental studies have explored this problem and have provided quantitative understanding. A numerical analysis of a wind turbine operating over a forest by Schröttle et al. [19] using large eddy simulations (LESs) showed faster wake recovery and vertical asymmetry in the wake, and forests may enable tighter spacing of wind turbine arrays. However, LESs of forest effects on large wind turbine arrays by Agafonova et al. [20] showed comparatively shorter, but wider, turbine wakes may be induced in forest terrains. They pointed out that stronger mean shear and higher turbulence intensity may reduce turbine life span. Agafonova [21] also noted that turbine arrays placed in a forest incurred a significant power loss as compared to the non-forest case; improper blade pitch of the turbines was determined as a major cause of the reduced power performance. LES investigation by Nebenführ and Davidson [22] showed fatigue load on a wind turbine is larger in the boundary layer developed over a forest.

Experimental studies have particularly focused on continuous forested-like fetch and forest edge effects on wind turbine wake, among others. Rodrigo et al. [23] studied the flow over porous foam sections and the effects on wind turbines in a clear-cut and noted a significant increase in turbulence, wind velocity, and wind shear leading to a decrease in energy output. They suggested that the clearance between the turbine rotor and the ground should be at least twice the height of the forest when the wind is perpendicular to the clear-cut axis. If the roles are flipped, however, and a porous windbreak is introduced into a relatively flat 'plains-like' environment, the power gained from a wind turbine increases. Indeed, Tobin and Chamorro [24] found that the porosity of windbreaks plays a significant role in the power output enhancement of a wind turbine but has a minor effect on the power output of a very large wind farm. Odemark and Segalini [25] modeled a forest with cylindrical pins to test different forest densities and the effects of heterogeneous forest structures such as clearings. They also varied the hub height of the wind turbine to study its impact on turbine performance and found minor changes in the maximum power output. This suggests that effects imposed on the wind turbine power output from incoming forest canopy boundary layers are not strongly dependent on the forest's structure. Chougule et al. [26] investigated the wind characteristic and turbine load in forested and agricultural sites. They observed a much higher turbulent kinetic energy (TKE) dissipation rate over forestry landscapes. Another essential consideration can be gleaned from field experiments by Zendehbad et al. [27], who have shown considerable increases in turbulence intensity and aeroelastic tower deflection of wind turbines in a forested fetch as well as a significant energy loss in a forested fetch, as compared to unforested fetch.

Overall, forests are one type of terrain that offers untapped potential for wind energy; likewise, the changes in the local mean shear and turbulence may also induce distinct differences in the transport of scalars in forestry terrains. Despite the substantial progress on characterizing forest boundary layer and induced turbulence and the insights into wind turbine performance, the unsteady interaction between turbine and wake with forest-modulated turbulence and the effect of distinct energetic motions in wind turbines are still far from well understood and should be explored in detail to inform optimized operation and extend the life span of the units.

Here, we aim to contribute to understanding the flow over forest canopies and wind turbine wake interaction by exploring the turbulence statistics. Such a characterization is needed for, e.g., multi-criteria decision support systems on wind farm site selection within forestry terrains [28]. Section 2 describes the experimental setup, Section 3 discusses the common and distinct flow statistics of wind turbine wakes over forest canopies, and Section 4 summarizes the main conclusions.

2. Experimental Set-Up

Wind tunnel experiments were performed to characterize the effects of a forest-like canopy and associated density on the wake and power output fluctuations of a model wind turbine. The experiments were carried out in the Eiffel-type wind tunnel of the University of Illinois at Urbana-Champaign. The test section is 6.1 m long, 0.914 m wide, and 0.47 m high; the top wall is fully adjustable to set pressure gradients, which was minor in the experiments. Details on the wind tunnel can be found in Adrian et al. [29].

An active turbulence generator was placed at the beginning of the test section to induce high-turbulence levels on the order of 10% with a well-developed turbulence structure with an inertial subrange spanning two decades at the turbine location for the base turbulent boundary layer (TBL) case without the presence of forest; additional details are found in Cheng et al. [30]. The forest canopies consisted of regular arrays of $H = 40$ mm high model maple trees of 30 mm crown diameter, with a trunk height of 15 mm and a crown height of 25 mm. They were placed along the test section over a 13 mm thick foam in two regular staggered patterns with streamwise and spanwise spacing of $\Delta x = \Delta y = 80$ and 40 mm, henceforth the intermediate and dense forests; see details in Figure 1. The canopy arrangements resulted in porosity $\varphi = V_V/V_T$ of 0.65 and 0.88, where V_V is the void volume, and V_T is the total volume.

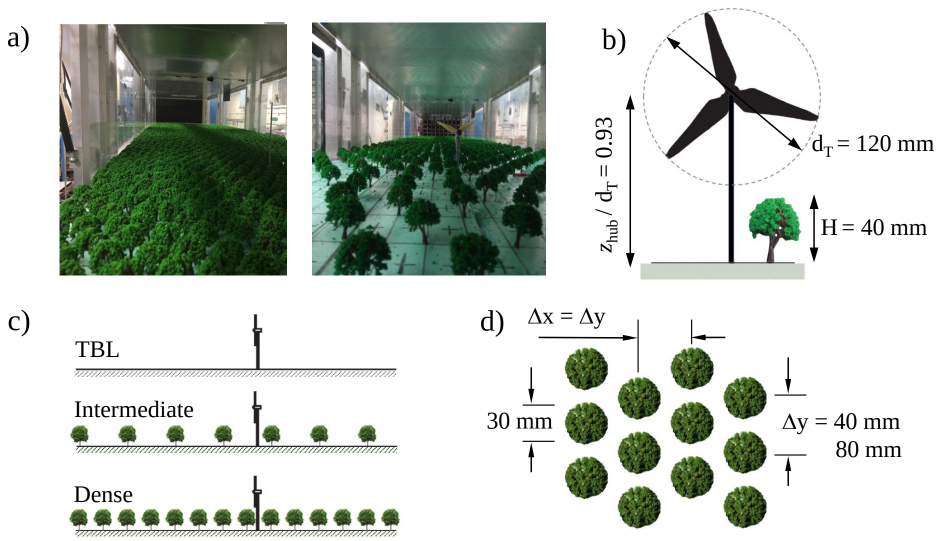

Figure 1. (**a**) Photographs of the wind tunnel with the intermediate and dense tree canopy models; (**b**) basic dimensions of the model wind turbine and tree; (**c**) side view of the scenarios; (**d**) top view of the geometrical layout of the tree arrangements.

The model turbine was fabricated following a design by the Sandia National Laboratories [31,32], with the 3D printed nacelle and blades using the Object Eden 350 machine at the University of Illinois Rapid-Prototyping Lab. The unit consists of a three-bladed horizontal-axis rotor of diameter $d_T = 120$ mm, a hub height of $z_{hub}/d_T = 0.93$ resulting in a ratio between the hub and tree heights of $z_{hub}/H = 2.8$, which provided a proper geometrical scaling. The loading system of the turbine model consisted of a Precision Microdrive 112-001 Micro core 12 mm diameter, which produced a rated power of $P_0 \sim 1$ W and allowed power measurements at high frequency. The angular velocity of the rotor ω was controlled by the resistance of the DC generator and operated with a tip-speed ratio of $\lambda = 0.5 d_T \omega / U_{hub} \approx 5$. The turbine power output was measured at 1 kHz for 300 s using a Measurement Computing USB-1608HS datalogger, and power was calculated from the applied resistance and the voltage measured across the generator terminals by a data acquisition system (DAQ). See Tobin et al. [33] for more details on model turbine features.

At the turbine location, the mean incoming flow velocity at hub height was set to $U_{hub} \approx 7.7$ m s^{-1}; specifically, 7.6 m s^{-1} and 7.8 m s^{-1} for the intermediate and dense canopy cases. This resulted in roughness lengths $z_o \approx 4.1$ mm and 4.4 mm with displacement heights of $h_0 = 9$ mm and 14 mm. As a complement, we include the case of the turbine in a canonical turbulent boundary layer with a boundary layer thickness of $\delta/z_{hub} \approx 2$, roughness length of $z_0 \approx 0.12$ mm. Figure 2 illustrates dimensionless vertical profiles of the incoming flow U/U_{hub}, turbulence intensity $I_u = \sigma_u/U_{hub}$, and kinematic shear stress $-\overline{u'w'}/U_{hub}^2$ of the boundary layers over the forests near the turbine location; the complementary case without a forest is also included for reference. Here, σ_u represents the standard deviation of the streamwise velocity fluctuations.

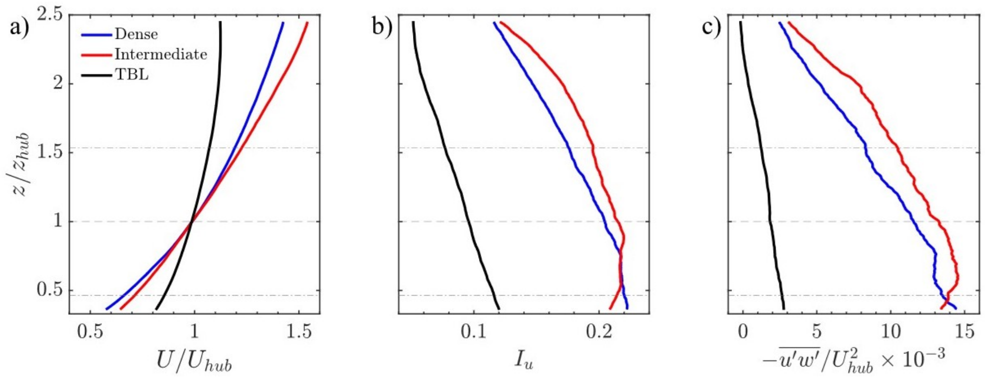

Figure 2. Characteristics of the incoming turbulent boundary layers. (**a**) Mean velocity U/U_{hub}, (**b**) streamwise turbulence intensity $I_u = \sigma_u/U_{hub}$, and (**c**) kinematic shear stress $-\overline{u'w'}/U_{hub}^2$.

Planar particle image velocimetry (PIV) was used to obtain velocity fields in four wall-normal fields of view (FOVs) at the rotor center plane; three of them in the wake within $x/d_T = [2.25,\ 3.25]$, [4.25, 5.25] and [6.25, 7.25], which shared the same vertical span of $z/z_{hub} \approx [0.4,\ 2.4]$; here, the origin of the coordinate system was set at the wall and coincident with the rotor plane. Another FOV was obtained upwind of the turbine; see details in Figure 3. In each FOV, 2000 image pairs were collected by an 11 MP (4000 pixels $\times$ 2672 pixels), 12 bit CCD camera at a 1 Hz sampling rate. Olive oil droplets of 1 µm ejected from Laskin nozzles were used to seed the flow, which was illuminated with a 1 mm laser sheet provided from a 250 mJ/pulse double-pulsed Quantel laser. The image pairs were interrogated using a recursive cross-correlation with the TSI Insight 4G software. The final, uniform vector grid spacing was $\Delta x = \Delta y = 0.97$ mm with an interrogation window of 24 pixels $\times$ 24 pixels with 50% overlap. Minor adjustments in the PIV setup including camera misalignment, light sheet plane alignment, resolution on the PIV setup, and PIV processing were revised, resulting in a standard deviation of approximately $1.2 \times 10^{-2} U_{hub}$ [34,35].

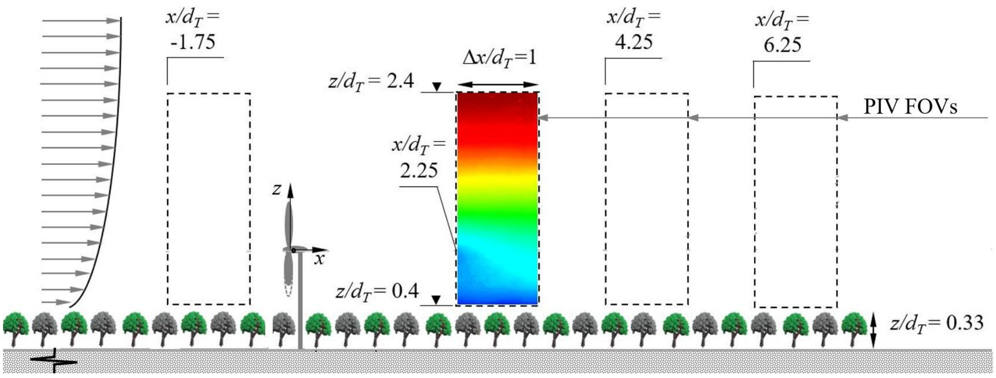

Figure 3. Basic schematic of the experimental setup illustrating two forest models with different tree density, PIV fields of view (FOVs), and basic dimensions.

3. Results

This section discusses the impact of the forest-like canopy and its density in the wind turbine wake statistics and turbulent transport above the forest canopy in the near and intermediate wake regions. The case without trees is used for selected comparison.

3.1. Mean Wake Characteristics

Inspection of the time-averaged streamwise velocity fields, $U(x/d_T, y/d_T = 0, z/d_T)/U_{hub}$, of the incoming flow and wake of the wind turbine over the intermediate and dense canopies, illustrated in the four fields of view in Figure 4, reveals minor differences but a substantial departure from canonical scenarios in a turbulent boundary layer over rough, flat terrain; see, e.g., [30,32,36].

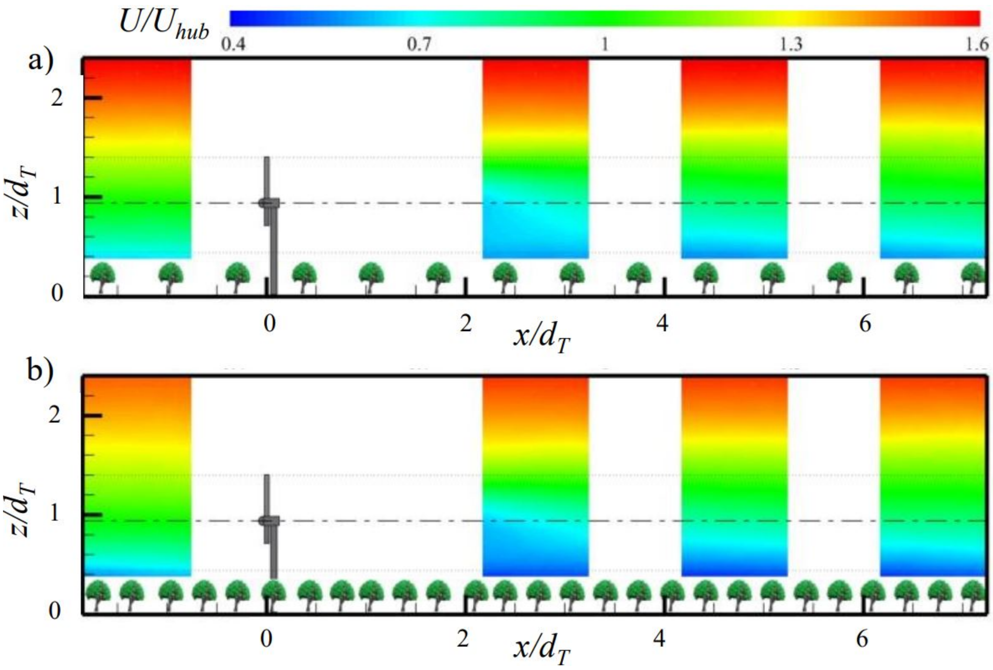

Figure 4. Time-averaged streamwise velocity distributions, $U(x, y = 0, z)/U_{hub}$, above the (**a**) intermediate and (**b**) dense canopies. The horizontal lines indicate the location of the hub, top and bottom tips of the turbine.

A closer look at the relative velocity deficit at selected streamwise locations, $\Delta U = U_{inc}(z/d_T) - U(x/d_T, z/d_T)$, is provided in Figure 5, where U_{inc} is the incoming boundary layer velocity profile. This figure shows that the velocity deficit within heights coinciding with the top and bottom tips is lower in the intermediate canopy scenario. The difference in

ΔU is larger in the intermediate wake region as the rotor strongly dominates the near wake. The larger inter-tree space promotes flow instability and, consequently, enhanced turbulent exchange; such exchange should approach a wall boundary layer case with increasing canopy density with very packed trees.

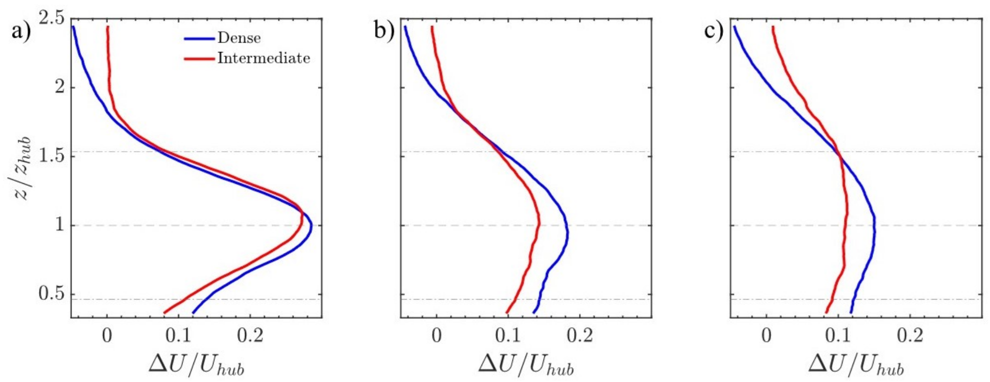

Figure 5. Vertical profiles of the time-averaged streamwise velocity deficit in the turbine wake, $\Delta U = U_{inc}(z) - U(x, y = 0, z)$, at x/d_T = (**a**) 3; (**b**) 5; (**c**) 7. The horizontal lines indicate the location of the hub, top and bottom tips of the turbine.

It is worth noting the similar ΔU distributions over the rotor area of the two cases in the near wake at $x/d_T = 3$ shown in Figure 5. Figure 6 illustrates the normalized turbine hub height velocity as a function of streamwise distance. As the near wake characteristics are largely affected by the presence of the turbine, the velocity profiles exhibit minor differences between the canopies; relatively large differences downwind as the effect of the forest terrain dominates over the turbine at distances $x/d_T \gtrsim 4$. It is also worth mentioning that the hub height flow recovery in the turbine wake in both cases is faster than that with a canonical TBL. For instance, $U/U_{hub} \approx 0.8$ and 0.6 [30,32] over the forest and TBL cases at $x/d_T \sim 4$.

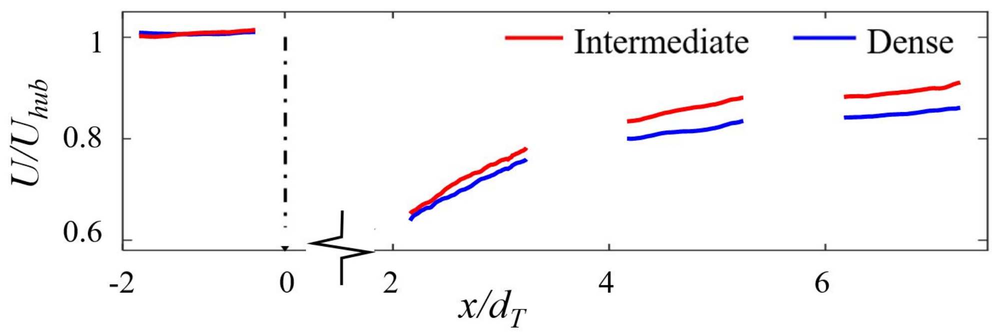

Figure 6. Non–dimensional hub height streamwise velocity profiles, U/U_{hub}, over the intermediate and dense forest canopies.

3.2. Turbulence Statistics

Bulk turbulence statistics reveal a relatively minor impact between the two forest densities in the turbine wake. In particular, Figure 7 shows the streamwise, $I_u = \sigma_u/U_{hub}$, wall-normal, $I_w = \sigma_w/U_{hub}$, turbulence intensity and the kinematic shear stress $-\overline{u'w'}/U_{hub}^2$ distributions with an iso-contour corresponding to their hub height values. Here, σ_i denotes the standard deviation of the $i-$velocity velocity fluctuations.

The I_u distribution exhibits larger values around the turbine top tip, where shear layer instability and tip vortices dominate that region [37,38]. Within this region, maximum values are roughly $x/d_T \sim 5$ for turbines placed within TBL [30,32], whereas it occurs closer to the turbine at roughly $x/d_T \sim 2$, indicating more energetic instability mechanisms under higher background turbulence. Bulk distributions of the kinematic shear stress exhibit shared features; however, the differences in the magnitudes may reveal distinct modulation of the sweep and ejection near the top of the canopies that interact with the wake. This is explored as follows.

The so-called quadrant hole analysis is performed to understand better the turbulence modulated by the forest–turbine interaction. Here, the quadrant-hole analysis is modified from those used in Lu and Willmarth [5], where the velocity fluctuations are decomposed into four quadrant domains. Each quadrant indicates the strength of certain events in the flow, where the second and fourth quadrants represent sweeps and ejections, whereas the first and third quadrants denote the outward and inward interactions.

The parameter H, also referred to as hyperbolic hole, splits regions with hyperbolic curves defined by $|u'w'| = H|\overline{u'w'}|$. The hole size H here is defined as the percentage of the total Reynolds shear stress following Yue et al. [10]. The mean quadrant events as a function of hole size H can then be defined as

$$S_{i,H} = \frac{1}{T}\int_0^T u'(x,z,t)w'(x,z,t)I_{i,H,t}(u',w')dt \quad (1)$$

with i indicating events of a specific quadrant and T is the sampling period for the velocity fluctuations. The piecewise function $I_{i,H,t}$ is introduced for conditional sampling, where

$$I_{i,H,t}(u',w') = \begin{cases} 1, & \text{for } (u',w') \text{ in quadrant } i \text{ and } |u'w'| \geq H\left|\overline{u'w'}\right| \\ 0, & \text{otherwise .} \end{cases} \quad (2)$$

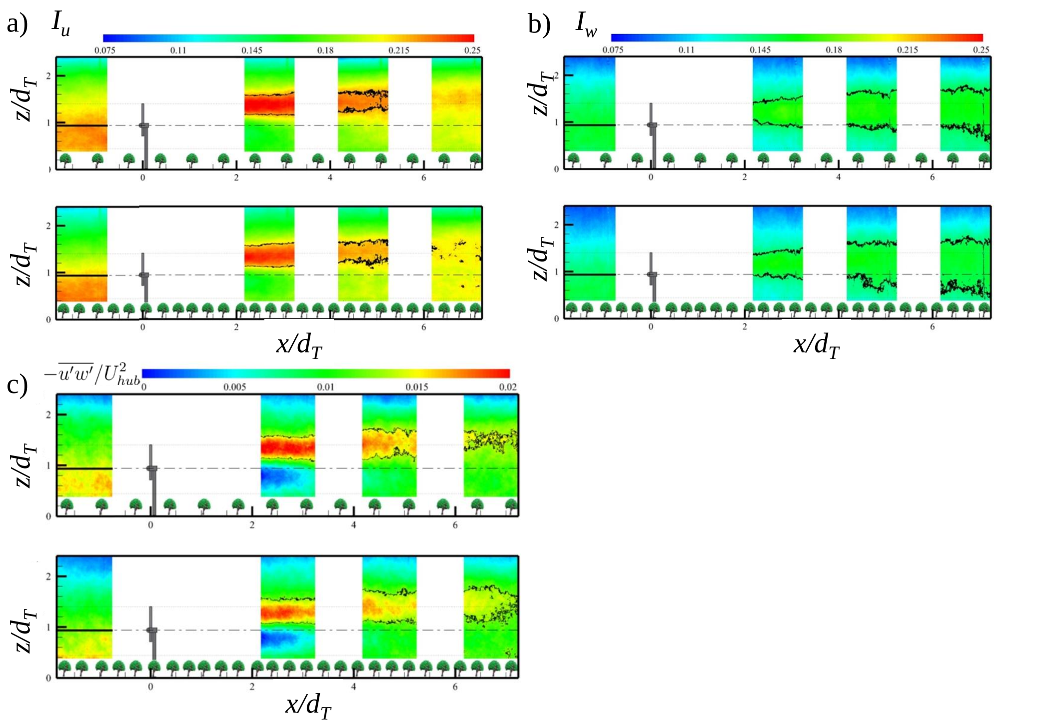

Figure 7. Turbulence intensity of the (**a**) streamwise, $I_u = \sigma_u/U_{hub}$, and (**b**) vertical, $I_w = \sigma_w/U_{hub}$, velocity components; (**c**) kinematic shear stress, $-\overline{u'w'}/U_{hub}^2$. The top subfigure in each case denotes the intermediate forest and the bottom subfigure the dense forest case, as indicated by the tree drawing. Iso-contours denote the values to those of the incoming flow at the hub height.

The quadrant fraction of the turbulent stresses can be calculated as $S_{i,H}^f = S_{i,H}/S$, where S is the mean stress $|\overline{u'w'}|$. Figure 8 shows $S_{i,H}^f$ as a function of H at two elevations; one near the wall at $z'/z_{hub} \approx 0.11$, where z' is the relative height defined with respect to the topography top and another at the turbine top tip, $z/z_{hub} = 1.6$. Interestingly, all three topographies exhibit a similar $S^f_{i,H}$ at the lower elevation near the wall and canopy top in the incoming boundary layer flow. However, an opposite trend occurred between the TBL and the forestry terrains at $z/z_{hub} = 1.6$. The TBL scenario shows a significant increase in the $Q2$ fraction, leading to ejection-dominated events, but forestry cases are sweep-dominated there, similar to the findings of Yue et al. [10]; this implies fast-moving downward fluctuations produced by the forests. It also shows that the trees modulate the structure of the Reynolds stress more significantly away from the canopy top, inducing a non-negligible interaction with the wake. The sweep–ejection dynamics are known to be modified by plant canopies due to the additional drag induced by the plants [3].

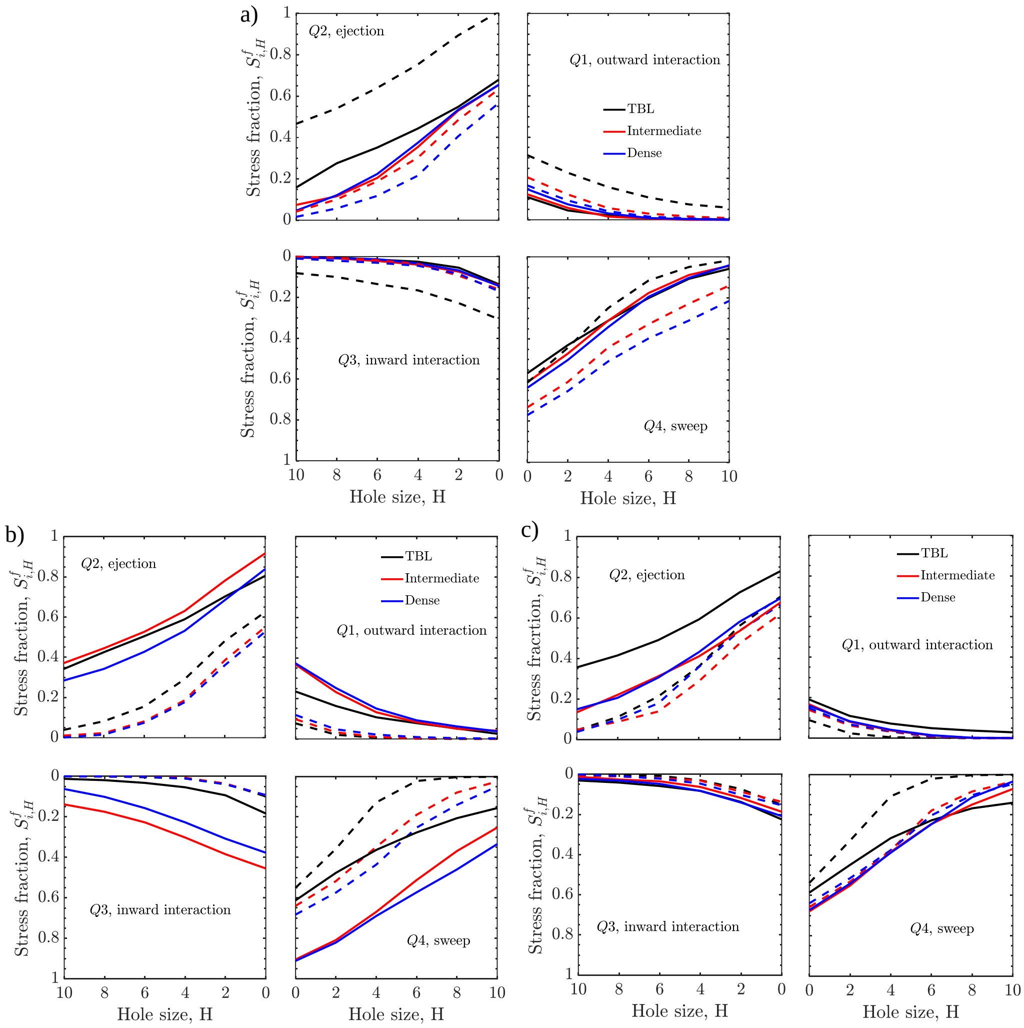

Figure 8. Kinematic shear stress fractions $S^f_{i,H}$ versus hole size, H, at $z/z_{hub} \approx 0.11$ (solid lines) and $z/z_{hub} = 1.6$ (dashed lines) above the forest canopies at (**a**) incoming boundary layer, (**b**) $x/d_T = 3$ and (**c**) $x/d_T = 6.5$.

Insight on the turbine–forest interaction is given in Figure 9b, where all near-wall quadrants show a higher fraction compared to those at the hub height due to stronger $Q1$ and $Q3$ events. The turbine wake redistributes turbulent structures and evens out the quadrant distribution along the vertical. This is better illustrated with the sweep-to-ejection ratio, $Q4/Q2$, shown in Figure 9 as a function of streamwise distance from the turbine. Comparatively close $Q4/Q2$ ratios between the near wall and top tip location occur in the near wake (Figure 9(b1,b2)) by comparing to the incoming boundary layer (Figure 9(a1,a2)). However, this feature is noted only in the TBL case in the intermediate wake region at $x/d_T \approx 6.5$ due to the higher $Q2$ near the wall and lower $Q4$ at the top tip

(Figure 8c). Relatively large separation similar to those observed in the incoming flow is shown in the intermediate wake of the forest canopies. It is also worth noting that the TBL $Q4$ fraction at $z/z_{hub} = 1.6$ in Figure 9b,c demonstrates a sharper decrease as the hyperbolic hole increases; this indicates that the turbine filters large-scale structures in the TBL and amplifies small-scale ones as pointed out in Chamorro et al. [39]. However, this is not the case for turbines placed within forest terrain, where the $dS_{f_{Q4,H}}/dH$ slope is similar to that observed in the incoming flow. All these observations of the quadrant-hole analysis offer information about the temporal structure of the turbulent momentum transfer [40] and demonstrate a strong role of forests in modulating the turbulent structure in the near and intermediate wake regions, which is consistent with the results shown in Section 3.1 and in line with those observed for turbine wake under high background turbulence discussed in Jin et al. [41].

Inspection of the probability distribution functions (PDFs) of the normalized streamwise velocity fluctuation u'/σ_u in Figure 10 further shows the signature of velocity fluctuation structure. Bimodal shapes with peaks near $\pm 0.6\sigma_u$ characterize the incoming boundary layer near the wall, similar to those reported by Laskari et al. [42], indicating horizontal sloshing motions near the canopies [3]. The forest terrains have a more evenly distributed u' showing the footprint of multi-scale structures. At the higher elevation, $z/z_{hub} = 1.6$, these trends skew towards the negative side for TBL and toward slightly positive for both forest cases. It shows that the forest mitigates the influence of the upwind draft motions inducing $Q4$ and $Q2$ dominated events. The modulation of the turbine is evidenced in the near wake (Figure 10b), where the bimodal shape changes to a more Gaussian-like distribution. The far wake structure shows a combination of the bimodal characteristic of the coherent structures from the boundary layer and those created from the turbine. The forest terrain cases are subjected to stronger motions and thus show a distribution closer to those in the incoming boundary layer at $x/d_T \approx 6.5$.

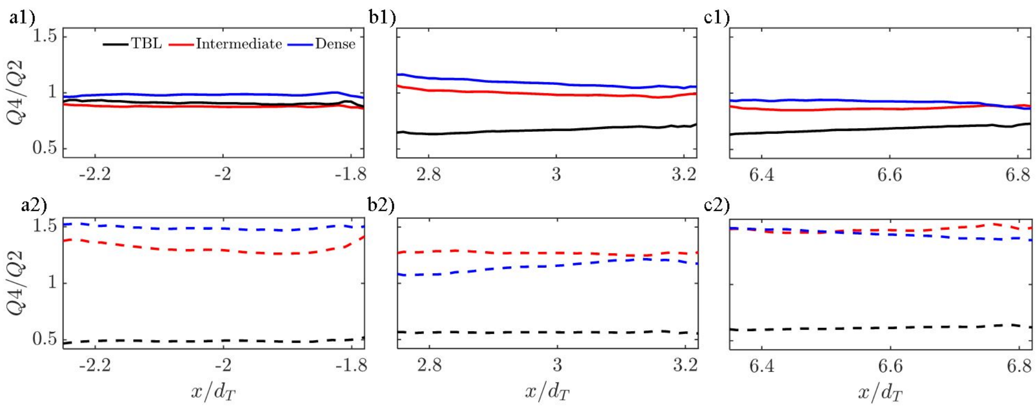

Figure 9. Ratio of total contribution of sweep ($Q4$) and ejection ($Q2$) events in the (**a**) incoming flow, (**b**) $x/d_T = 3$, and (**c**) $x/d_T = 6.5$ at $\Delta z/z_hub = 0.11$ (solid lines) above the surface and $z/z_{hub} = 1.6$ (dashed lines).

Finally, bulk assessment on the modulation of the forest on the turbine performance can be obtained by measuring the relative turbine performance and power fluctuations. In particular, Figure 11 shows the ratio between the mean power output, $\overline{P}$, and the cube of the incoming velocity at hub height, U^3_{hub}, as a first-order estimation of the forest-modulated impact on the power coefficient or performance; the TBL scenario is also added for comparison. Note that $\overline{P}/U^3_{hub}$ is lower in the turbine over the forest canopies. This is indicative of a lower turbine performance associated with lower blade performance, likely due to increased local flow separation promoted by the enhanced turbulence levels of the incoming flow (Figure 2b). This shows that local flow control on the blade and real-time rotor control are two engineering challenges that need more attention in turbines operating in high-turbulence flows.

As expected, the power fluctuations are higher in the forest scenarios due to the higher turbulence, as velocity fluctuations of the incoming flow are a central source of power fluctuations, e.g., [43]; only minor differences in σ_P between the forests are obtained due to the similar turbulence (Figure 2). Inspection of the power output structure shown in Figure 11b with the compensated spectra shows that the power fluctuations in the forest cases are dominated by comparatively high energy content in the smaller scales, consistent with the smaller turbulence length scale observation in Agafonova et al. [20]. This explains the reduced bulk power fluctuation ratio between forest cases and the TBL case (i.e., $\sigma_{u,forest}/\sigma_{u,TBL} > \sigma_{P,forest}/\sigma_{P,TBL}$) seen in Figure 11a, as Chamorro et al. [44] pointed out that power fluctuations of turbines are insensitive to the upwind coherent structures smaller than the rotor size.

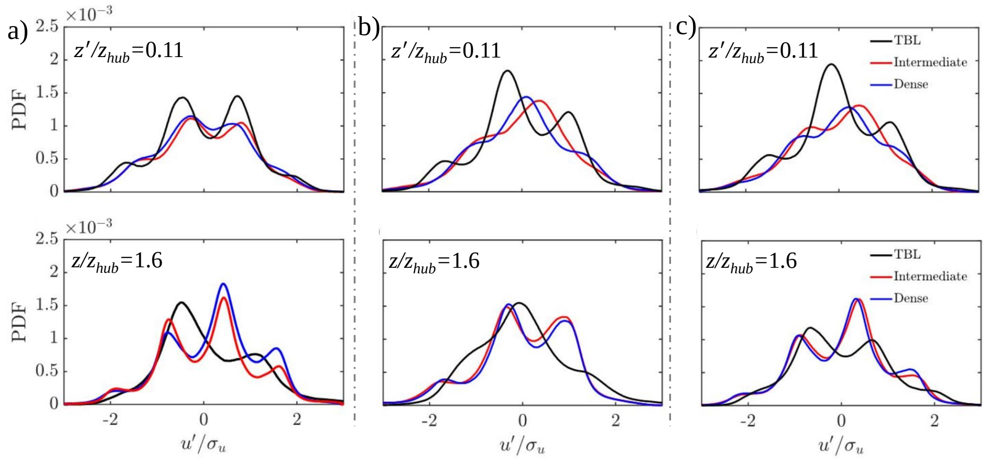

Figure 10. Probability density functions, PDFs, of the normalized streamwise velocity fluctuations, u'/σ_u, at (**a**) incoming flow, (**b**) $x/d_T = 3$, and (**c**) $x/d_T = 6.5$; z' is the relative height with respect to the topography top.

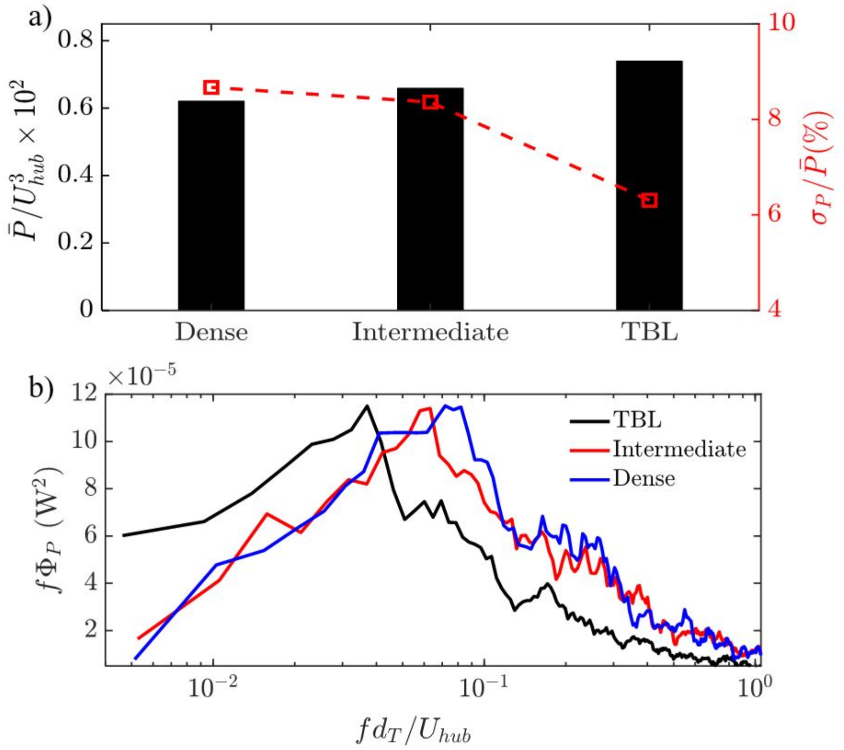

Figure 11. (**a**) Ratio of the time-averaged power output and U_{hub}^3, and power output intensity, $\sigma_P/\overline{P}$; (**b**) compensated power output spectra $f\Phi_P$.

4. Conclusions

The experiments with a model wind turbine operating within two forest terrains with different densities showed similarities and distinct departures with the case of a turbine in a canonical turbulent boundary layer. As expected, the presence of forest produced stronger background turbulence, which resulted in faster wake recovery. The forests imposed a non-negligible effect on the mean turbine wake and associated second-order statistics compared to a TBL scenario. The forest density imposed a minor impact on the bulk features of the wake, but the less dense forest induced a faster flow recovery in the wake.

Close inspection of the Reynolds stress with quadrant-hole analysis using the so-called hyperbolic hole provided insight into the forest modulation on the flow past the turbine. In particular, it shows a strong influence of the forests relatively far above the canopy at a height coincident with the turbine top tip. That region exhibited sweep-dominated events, which are distinct from the ejection-dominated ones observed with turbines in TBL. Additionally, the strong background turbulence induced by the forests reduced the rotor modulation in the near wake region, namely $x/d_T \lesssim 3$. In the intermediate wake at $x/d_T \sim 6-7$, the quadrant fraction resembled a similar distribution of the incoming flow. In contrast, the impact of the rotor in the TBL, in general, covers an extended region downwind.

The results provide basic information that may be incorporated in, e.g., multi-criteria decision support systems in the context of location selection [28,45], layout design [46], and operation of wind farms [47] within forestry terrains. The study mainly focused on exploring the near to intermediate wake of a model wind turbine placed in a developed forest canopy boundary layer. The canopy layouts are composed of regularly spaced trees in staggered patterns, which deviate from natural forests that exhibit a wide range of height and layout heterogeneity. However, these may induce relatively minor effects in dense forests [25]. However, that may not be the case in low-density forests; the associated impact on wind turbines and wind farms should be assessed in detail.

Future studies will expand current work in a wider forest density range and include additional parameters such as the number of turbines, topography heterogeneity, and pressure gradients.

Author Contributions: Experiments, S.C. and M.E.; methodology, S.C., M.E., and L.P.C.; formal analysis, all; writing—original draft preparation, S.C. and L.P.C.; supervision and project administration, L.P.C.; writing—review and editing, L.P.C. All authors have read and agreed to the published version of the manuscript.

Funding: This research received no external funding.

Institutional Review Board Statement: Not applicable.

Informed Consent Statement: Not applicable.

Data Availability Statement: The data of this study are available from the corresponding author upon reasonable request.

Acknowledgments: This work was supported by the Department of Mechanical Science and Engineering, University of Illinois at Urbana-Champaign.

Conflicts of Interest: The authors declare no conflict of interest.

Abbreviations

TBL	Turbulent Boundary Layer
PIV	Particle Image Velocimetry
FOV	Field of View
TKE	Turbulence Kinetic Energy
PDF	Probability Density Function

References

1. Alfredsson, P.H.; Segalini, A. *Introduction Wind Farms in Complex Terrains: An Introduction*; The Royal Society Publishing: London, UK, 2017.
2. Baldocchi, D.D.; Meyers, T.P. Turbulence structure in a deciduous forest. *Bound.-Layer Meteorol.* **1988**, *43*, 345–364. [CrossRef]
3. Finnigan, J. Turbulence in plant canopies. *Annu. Rev. Fluid Mech.* **2000**, *32*, 519–571. [CrossRef]
4. Cava, D.; Katul, G.; Scrimieri, A.; Poggi, D.; Cescatti, A.; Giostra, U. Buoyancy and the sensible heat flux budget within dense canopies. *Bound.-Layer Meteorol.* **2006**, *118*, 217–240. [CrossRef]
5. Lu, S.; Willmarth, W. Measurements of the structure of the Reynolds stress in a turbulent boundary layer. *J. Fluid Mech.* **1973**, *60*, 481–511. [CrossRef]
6. Poggi, D.; Katul, G.; Albertson, J. Momentum transfer and turbulent kinetic energy budgets within a dense model canopy. *Bound.-Layer Meteorol.* **2004**, *111*, 589–614. [CrossRef]
7. Poggi, D.; Porporato, A.; Ridolfi, L.; Albertson, J.; Katul, G. The effect of vegetation density on canopy sub-layer turbulence. *Bound.-Layer Meteorol.* **2004**, *111*, 565–587. [CrossRef]
8. Zhu, W.; Van Hout, R.; Katz, J. PIV measurements in the atmospheric boundary layer within and above a mature corn canopy. Part II: Quadrant-hole analysis. *J. Atmos. Sci.* **2007**, *64*, 2825–2838. [CrossRef]
9. Lopes, J.V.P.; Palma, J.; Lopes, A.S. Modelling the flow within forests: The canopy-related terms in the Reynolds-averaged formulation. *J. Fluid Mech.* **2021**, *910*. [CrossRef]
10. Yue, W.; Meneveau, C.; Parlange, M.B.; Zhu, W.; Van Hout, R.; Katz, J. A comparative quadrant analysis of turbulence in a plant canopy. *Water Resour. Res.* **2007**, *43*. [CrossRef]
11. Arnqvist, J.; Segalini, A.; Dellwik, E.; Bergström, H. Wind statistics from a forested landscape. *Bound.-Layer Meteorol.* **2015**, *156*, 53–71. [CrossRef]
12. Kuwata, Y.; Suga, K. Lattice Boltzmann direct numerical simulation of interface turbulence over porous and rough walls. *Int. J. Heat Fluid Flow* **2016**, *61*, 145–157. [CrossRef]
13. Gómez-de Segura, G.; García-Mayoral, R. Turbulent drag reduction by anisotropic permeable substrates—Analysis and direct numerical simulations. *J. Fluid Mech.* **2019**, *875*, 124–172. [CrossRef]
14. Irvine, M.; Gardiner, B.; Hill, M. The evolution of turbulence across a forest edge. *Bound.-Layer Meteorol.* **1997**, *84*, 467–496. [CrossRef]
15. Bailey, B.N.; Stoll, R. The creation and evolution of coherent structures in plant canopy flows and their role in turbulent transport. *J. Fluid Mech.* **2016**, *789*, 425–460. [CrossRef]
16. Placidi, M.; Ganapathisubramani, B. Turbulent flow over large roughness elements: Effect of frontal and plan solidity on turbulence statistics and structure. *Bound.-Layer Meteorol.* **2018**, *167*, 99–121. [CrossRef] [PubMed]
17. Pietri, L.; Petroff, A.; Amielh, M.; Anselmet, F. Turbulence characteristics within sparse and dense canopies. *Environ. Fluid Mech.* **2009**, *9*, 297. [CrossRef]
18. Sharma, A.; García-Mayoral, R. Turbulent flows over sparse canopies. *J. Phys. Conf. Ser.* **2018**, *1001*, 012012. [CrossRef]
19. Schröttle, J.; Piotrowski, Z.; Gerz, T.; Englberger, A.; Dörnbrack, A. Wind turbine wakes in forest and neutral plane wall boundary layer large-eddy simulations. *J. Phys. Conf. Ser.* **2016**, *753*, 032058. [CrossRef]
20. Agafonova, O.; Avramenko, A.; Chaudhari, A.; Hellsten, A. Effects of the canopy created velocity inflection in the wake development in a large wind turbine array. *J. Phys. Conf. Ser.* **2016**, *753*, 032001. [CrossRef]
21. Agafonova, O. *A Numerical Study of Forest Influences on the Atmospheric Boundary Layer and Wind Turbines*; Lappeenranta University of Technology: Lappeenranta, Finland, 2017.
22. Nebenführ, B.; Davidson, L. Prediction of wind-turbine fatigue loads in forest regions based on turbulent LES inflow fields. *Wind Energy* **2017**, *20*, 1003–1015. [CrossRef]
23. Rodrigo, J.S.; Van Beeck, J.; Dezsö-Weidinger, G. Wind tunnel simulation of the wind conditions inside bidimensional forest clear-cuts. Application to wind turbine siting. *J. Wind. Eng. Ind. Aerodyn.* **2007**, *95*, 609–634. [CrossRef]
24. Tobin, N.; Chamorro, L.P. Windbreak effects within infinite wind farms. *Energies* **2017**, *10*, 1140. [CrossRef]
25. Odemark, Y.; Segalini, A. The effects of a model forest canopy on the outputs of a wind turbine model. *J. Phys. Conf. Ser.* **2014**, *555*, 012079. [CrossRef]
26. Chougule, A.; Mann, J.; Segalini, A.; Dellwik, E. Spectral tensor parameters for wind turbine load modeling from forested and agricultural landscapes. *Wind Energy* **2015**, *18*, 469–481. [CrossRef]
27. Zendehbad, M.; Chokani, N.; Abhari, R.S. Impact of forested fetch on energy yield and maintenance of wind turbines. *Renew. Energy* **2016**, *96*, 548–558. [CrossRef]
28. Asadi, M.; Pourhossein, K. Wind farm site selection considering turbulence intensity. *Energy* **2021**, *236*, 121480. [CrossRef]
29. Adrian, R.J.; Meinhart, C.D.; Tomkins, C.D. Vortex organization in the outer region of the turbulent boundary layer. *J. Fluid Mech.* **2000**, *422*, 1–54. [CrossRef]
30. Cheng, S.; Jin, Y.; Chamorro, L.P. Wind Turbines with Truncated Blades May Be a Possibility for Dense Wind Farms. *Energies* **2020**, *13*, 1810. [CrossRef]
31. Shiu, H.; Van Dam, C.; Johnson, E.; Barone, M.; Phillips, R.; Straka, W.; Fontaine, A.; Jonson, M. A design of a hydrofoil family for current-driven marine-hydrokinetic turbines. In *International Conference on Nuclear Engineering*; American Society of Mechanical Engineers: New York, NY, USA, 2012; Volume 44984, pp. 839–847.

32. Tobin, N.; Hamed, A.M.; Chamorro, L.P. An experimental study on the effects ofwinglets on the wake and performance of a modelwind turbine. *Energies* **2015**, *8*, 11955–11972. [CrossRef]
33. Tobin, N.; Hamed, A.M.; Chamorro, L.P. Fractional flow speed-up from porous windbreaks for enhanced wind-turbine power. *Bound.-Layer Meteorol.* **2017**, *163*, 253–271. [CrossRef]
34. Raffel, M.; Willert, C.E.; Scarano, F.; Kähler, C.J.; Wereley, S.T.; Kompenhans, J. PIV uncertainty and measurement accuracy. In *Particle Image Velocimetry*; Springer: Berlin/Heidelberg, Germany, 2018; pp. 203–241.
35. Adrian, R.J.; Westerweel, J. *Particle Image Velocimetry*; Number 30; Cambridge University Press: Cambridge, UK, 2011.
36. Fu, S.; Jin, Y.; Zheng, Y.; Chamorro, L.P. Wake and power fluctuations of a model wind turbine subjected to pitch and roll oscillations. *Appl. Energy* **2019**, *253*, 113605. [CrossRef]
37. Chamorro, L.P.; Porté-Agel, F. A wind-tunnel investigation of wind-turbine wakes: Boundary-layer turbulence effects. *Bound.-Layer Meteorol.* **2009**, *132*, 129–149. [CrossRef]
38. Odemark, Y. Wakes Behind Wind Turbines-Studies on Tip Vortex Evolution and Stability. Ph.D. Thesis, KTH Royal Institute of Technology, Stockholm, Sweden, 2012.
39. Chamorro, L.; Guala, M.; Arndt, R.; Sotiropoulos, F. On the evolution of turbulent scales in the wake of a wind turbine model. *J. Turbul.* **2012**, *13*, N27. [CrossRef]
40. Wallace, J.M. Quadrant analysis in turbulence research: History and evolution. *Annu. Rev. Fluid Mech.* **2016**, *48*, 131–158. [CrossRef]
41. Jin, Y.; Liu, H.; Aggarwal, R.; Singh, A.; Chamorro, L.P. Effects of freestream turbulence in a model wind turbine wake. *Energies* **2016**, *9*, 830. [CrossRef]
42. Laskari, A.; de Kat, R.; Hearst, R.J.; Ganapathisubramani, B. Time evolution of uniform momentum zones in a turbulent boundary layer. *J. Fluid Mech.* **2018**, *842*, 554–590. [CrossRef]
43. Milan, P.; Wächter, M.; Peinke, J. Turbulent character of wind energy. *Phys. Rev. Lett.* **2013**, *110*, 138701. [CrossRef]
44. Chamorro, L.P.; Lee, S.J.; Olsen, D.; Milliren, C.; Marr, J.; Arndt, R.; Sotiropoulos, F. Turbulence effects on a full-scale 2.5 MW horizontal-axis wind turbine under neutrally stratified conditions. *Wind Energy* **2015**, *18*, 339–349. [CrossRef]
45. Kazak, J.; Van Hoof, J.; Szewranski, S. Challenges in the wind turbines location process in Central Europe—The use of spatial decision support systems. *Renew. Sustain. Energy Rev.* **2017**, *76*, 425–433. [CrossRef]
46. Sunak, Y.; Höfer, T.; Siddique, H.; Madlener, R.; De Doncker, R.W. *A GIS-Based Decision Support System for the Optimal Siting of Wind Farm Projects*; Universitätsbibliothek der RWTH Aachen: Aachen, Germany, 2015.
47. Lee, A.H.; Chen, H.H.; Kang, H.Y. Multi-criteria decision making on strategic selection of wind farms. *Renew. Energy* **2009**, *34*, 120–126. [CrossRef]